Quantitative Thermal Imaging for Plasmonic Photothermal Therapy

Shiou-Han Wang[1,2] Chen-Wei Wei[3] Shiou-Hwa Jee[2] Pai-Chi Li[1,3,*]

[1]*Graduate Institute of Biomedical Electronic and Bioinformatics, National Taiwan University, Taipei 100, Taiwan, ROC*
[2]*Department of Dermatology, National Taiwan University Hospital and National Taiwan University College of Medicine, Taipei 100, Taiwan, ROC*
[3]*Department of Electrical Engineering, National Taiwan University, Taipei 100, Taiwan, ROC*

Received 13 Jun 2010; Accepted 7 Sep 2010; doi: 10.5405/jmbe.810

Abstract

Continuous-wave (CW) laser-induced thermotherapy (LIT) can heat tumors to above 42℃ and lead to tumor destruction. During LIT, antibody-conjugated gold nanorods (AuNRs) can bind to tumor tissue and improve therapeutic efficacy when implementing plasmonic photothermal therapy (PPTT). This study uses a noninvasive photoacoustic (PA) technique to monitor temperature during PPTT. A pulsed laser is used to generate the PA signal. AuNRs are used to further increase the PA-signal contrast during PA imaging. Ultrasound (US) is combined with PA imaging for anatomical imaging. The bimodal system of US and PA imaging is superior to conventional systems at locating tumors and recognizing nanoparticles, and facilitates the selection of an optimal treatment plan. This technique allows temperature to be monitored in real-time during therapy, thereby ensuring both safety and efficacy. The technique is based on the fact that the Grüneisen parameter (which determines the acoustic pressure amplitude) is linearly related to the temperature of soft tissue. The results of a phantom study show that the temperature and the thermal mapping of the laser-irradiated area can be exactly measured and drawn quantitatively. Under the ANSI Z136.1 safety guidelines, inducing thermotherapy without AuNRs is difficult with low laser power density. However, by using specific antibody-conjugated AuNRs, targeted thermotherapy can be implemented selectively. An *in vivo* study is performed to confirm the feasibility of the proposed technique. A quantitative thermal image of the laser-irradiated tumor shows that the temperature is above 45℃, indicating the induction of thermal therapy. The tumor after thermotherapy is examined histologically. The tumor architecture is destroyed whereas the peripheral and intratumor noncarcinoma cells are preserved despite also being irradiated by the CW laser. This indicates that antibody-conjugated AuNRs can facilitate targeted thermotherapy to selectively kill tumor cells. Both phantom and *in vivo* imaging results demonstrate that real-time quantitative thermal imaging is feasible for AuNR-assisted PPTT.

Keywords: Gold nanorods (AuNRs), Laser-induced thermotherapy (LIT), Photoacoustic (PA) effect, Plasmonic photothermal therapy (PPTT), Quantitative thermal imaging

1. Introduction

Thermal therapy is a kind of anticancer treatment in which the tumors are destroyed by being heated to above 42℃ for several to tens of minutes [1]. Many kinds of energy source can be used for thermal therapy, including radio frequencies, microwaves, ultrasound (US), and laser radiation [2]. Laser-induced thermotherapy applies laser energy to destroy carcinoma cells by coagulation necrosis [3]. Nanoparticles can also be used to enhance heat absorption at specific wavelengths determined by surface plasmon resonance (SPR), a technique called plasmonic photothermal therapy (PPTT) [1]. Temperature monitoring is essential for ensuring both the safety and efficacy of thermal therapy. In many applications, submillimeter spatial resolution with a temperature accuracy better than 1℃ is desirable [4].

Direct temperature monitoring with a thermocouple is the most straightforward technique, but it is invasive and thus generally not feasible. In addition, the temperature can only be monitored within a small region and the presence of the thermocouple can interfere with the treatment modality. These have prompted the development of noninvasive methods for temperature measurement. One example is infrared thermography, which can estimate the temperature in real-time with an accuracy of 0.1℃; however, its application is limited by its poor tissue penetration. Ultrasound is capable of real-time temperature monitoring at depth, but its accuracy and

* Corresponding author: Pai-Chi Li
Tel: +886-2-33663551; Fax: +886-2-83691354
E-mail: paichi@ntu.edu.tw

temperature range are limited [4-9]. Magnetic resonance imaging (MRI) can provide high resolution with adequate accuracy, but the acquisition time is too long for real-time applications [10-12].

Photoacoustic (PA) techniques have recently been widely investigated and applied to biology and medicine [13]. Applications include measurements of hemoglobin, real-time blood oxygen monitoring, brain functional and structural imaging, breast tumor imaging, and tumor angiogenesis. During cryotherapy and thermotherapy, PA techniques can be applied to measure tissue temperature [14,15]. Adequate spatial and temperature resolution have been demonstrated for ophthalmologic laser surgery [16,17] and photothermal cancer therapy [9,18]. Despite these achievements, quantitative PA thermal mapping has not been demonstrated *in vivo*.

2. Theory

2.1 Generation of a PA signal

Characterizing PA-signal generation requires several parameters to be defined. Let *c* denote the speed of sound. For enthalpy *h*, entropy *s*, pressure *p*, and volume *v*, the unit density is $\rho \equiv 1/v$, the temperature is $T \equiv (\partial h/\partial s)_P$, the heat capacity at a constant pressure is $C_P \equiv (\partial h/\partial T)_P$, and the thermal volume expansion coefficient is $\beta \equiv (\partial v/\partial T)_p / v$. For soft tissues, the state function of temperature is:

$$dT = (\partial T/\partial p)_s dp + (\partial T/\partial s)_p ds \tag{1}$$

and the state function of pressure is:

$$dp = (\partial p/\partial \rho)_s d\rho + (\partial p/\partial s)_\rho ds \tag{2}$$

These two functions can be respectively simplified to:

$$dT = T\beta C_p^{-1}\rho_0^{-1} dp + TC_p^{-1} ds \tag{3}$$

and

$$dp = c^2 d\rho + \rho_0 c^2 T\beta C_p^{-1} ds \tag{4}$$

From these equations, the pressure can be expressed as:

$$dp = c^2 d\rho + \rho_0 c^2 \beta dT \tag{5}$$

Density changes can be neglected during the generation of the PA signal, and so the first term in Eq. (5) can be modified as [19]:

$$dp = \rho_0 c^2 \beta dT \tag{6}$$

For a thermal system employing a pulsed laser, laser energy *E* can be expressed as:

$$E = \rho_0 v C_p \Delta T \tag{7}$$

where *E* is the product of fluence *F* and the cross section, and *v* is the irradiated volume. From the Beer-Lambert law, the variation of fluence is:

$$\delta F = -\mu_a F_0 e^{-\mu_a z} \delta z \tag{8}$$

where F_0 is the initial fluence, *z* is the penetration depth, and μ_a is the absorption coefficient of the medium. The pressure function can then be derived as [4]:

$$p(z) = \frac{\beta c^2}{C_p} \mu_a F_0 e^{-\mu_a z} \tag{9}$$

2.2 PA signal and temperature

The PA signal is generated by the pressure increase resulting from the absorption of pulsed laser energy. The dimensionless Grüneisen parameter, Γ, is related to the pressure by:

$$p(z) = \frac{\beta c^2}{C_p} \mu_a F_0 e^{-\mu_a z} = \Gamma \mu_a F(z) \tag{10}$$

For soft tissues, thermal expansion coefficient β is linearly proportional to the temperature within a range of 10 to 55℃ [9], and thus Γ is linearly proportional to the temperature [4]:

$$\Gamma = a + bT \tag{11}$$

where *a* and *b* are constants. Rewriting Eq. (10) as:

$$p(z) = (a + bT)\mu_a F_0 e^{-\mu_a z} \tag{12}$$

allows the temperature-pressure relationship to be expressed as:

$$T(z) = (a + bT_0(z))/b \cdot p(z)/p_0(z) + (T_0(z) - (a + bT_0(z))/b) \tag{13}$$

Equation (13) can then be simplified to:

$$T(z) = cp(z) + d \tag{14}$$

where $c = (a + bT_0(z))b^{-1}p_0(z)^{-1}$, d = −a/b, and T_0 and P_0 represent the initial temperature and pressure, respectively. Therefore, measuring the PA signal makes quantitative temperature mapping possible during thermotherapy.

3. Materials and methods

A custom-made PA transducer with a focal depth of 9.5 mm, a center frequency of 20 MHz, and a fractional bandwidth of 50% was used in experiments to assess the usefulness of the proposed technique. An optical fiber with a diameter of 600 μm (Thorlabs, Newton, NJ) was placed at the center of the transducer for coregistered laser irradiation (LOTIS TII, Minsk, Belarus) and acoustic detection.

A continuous-wave (CW) laser was used as the heat source for thermotherapy, and a pulsed laser was used to generate a PA signal for imaging. A laser power meter (Ophir Laser Measurement Group, North Logan, UT) was used to measure the energy of the laser system in order to normalize the results in the presence of laser instability.

Equation (14) was validated by performing experiments with agarose phantoms containing graphite in various concentrations. In vivo animal studies involved NOD-SCID male mice being subcutaneously inoculated with OECM1 oral squamous cell carcinoma. Gold nanorods (AuNRs) conjugated with anti-HER2 antibody ($AuNR_{800}$-anti-HER2), which have peak absorption at 800 nm, were injected subcutaneously (s.c.) into the tumor or intravenously (i.v.) into the tail vein of the mice. The tumor was subsequently irradiated by a CW diode

laser at 808 nm and 660 mW (ONSET Electro-optics, Taipei, Taiwan) for PPTT immediately and 24 hours after s.c. and i.v injections. The PA signals were generated simultaneously with a pulsed wavelength-tunable Ti:sapphire laser at 800 nm and 2.5 mJ/pulse, with a pulse duration of 16 ns (CF-125, SOLAR TII, Minsk, Belarus). A precision translation stage (HR8, Nanomotion, Yokneam, Israel) with a step size of 0.2 mm controlled by a motion controller (DMC-1842, Galil Motion Control, Rocklin, CA) was employed to position the transducer for cross-sectional PA imaging.

The detected PA signal was sent to a preamplifier (5077PR, Panametrics, Waltham, MA) and a 12-bit data acquisition card (CompuScope 12100, Gage, Lachine, QC, Canada) that was triggered by a photodetector (ET-2020, Electro-Optics Technology, Traverse City, MI) with a sampling rate of 200 MHz. These elements were controlled by LabVIEW® and MATLAB® software. A fine-needle thermocouple with 0.1°C accuracy (EDL NCF-06GS4TL3M, Danville, VA) and a digital multimeter (Model 189 True RMS Multimeter, Fluke, Everett, WA) were utilized to measure the temperature in the region of interest (ROI) (Fig. 1).

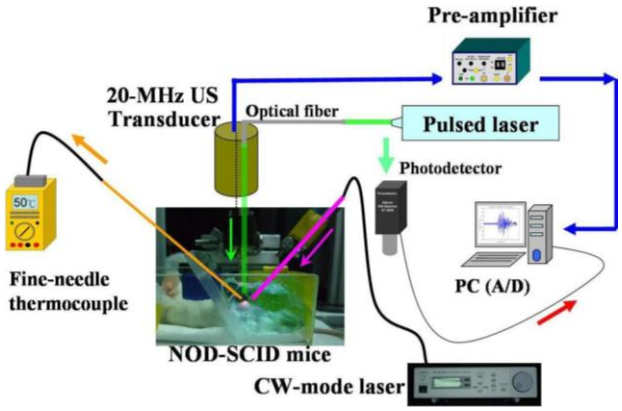

Figure 1. Experimental setup. In in vivo study, the subjects were NOD-SCID male mice inoculated with oral squamous cell carcinoma OECM1. The subjects are graphite in agarose gel in the phantom studies.

For the in vivo measurements, conjugated $AuNR_{800}$-anti-HER2 and $AuNR_{800}$-RGD4C nanoparticles contained anti-HER2 protein antibody and RGD (Arg-Gly-Asp) peptides (which have high affinity to blood vessels), respectively. The RGD peptide can specifically bind to the $\alpha_v\beta_3$ integrin on the membrane of endothelial cells where tumor angiogenesis is occurring [20]. The $\alpha_v\beta_3$ integrin acts as a marker of angiogenesis and can thus be used to monitor tumor growth [21,22].

4. Results and discussion

4.1 Temperature and absorption coefficient

In Eq. (10), laser fluence F_0 is set to a constant value and z is related to the focal depth of the transducer, and hence Grüneisen parameter Γ and absorption coefficient μ_a are the two remaining temperature-dependent parameters. It is assumed that the absorption coefficient is independent of temperature, and thus it can be assumed that there is a linear relationship between the Grüneisen parameter and temperature. An integrating sphere was used to validate this assumption (results not shown).

4.2 Thermal effects and the PA signal

Measurements were performed on several phantoms with various absorption coefficients. A highly linear relationship between the PA-signal amplitude and temperature was demonstrated. Figure 2 shows the results from a 0.80%-graphite phantom.

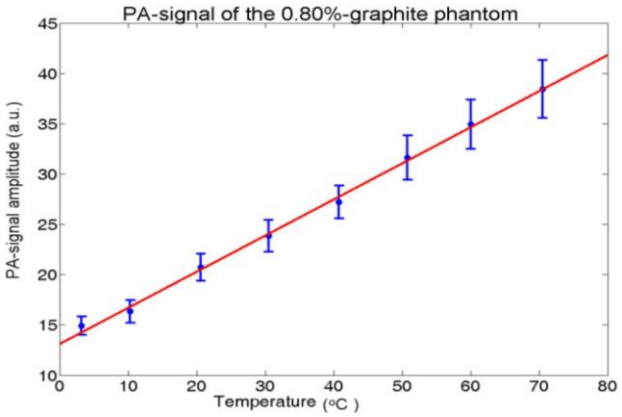

Figure 2. The relationship between temperature and the PA-signal amplitude from a 0.80%-graphite phantom was highly linear. Data are mean and SD values (n = 100).

During PPTT, the nanoparticles are irradiated with laser radiation at a specific wavelength, and electrons constituting the nanoparticles can be heated to thousands of Celcius within hundreds of picoseconds. This results in the macroscopic temperature being raised by tens of degrees Celsius [1]. Since temperature monitoring is essential for both efficacy and safety, the monitoring method has to exhibit a rapid response and allow monitoring over the entire treatment period.

Several tests were performed to validate the performance of the proposed system. As shown in Fig. 3(a), the PA-signal amplitude increases to its maximum level and then decreases to the baseline in less than 1 second after turning on and off the laser, respectively. Thermotherapy takes up to several tens of minutes, making long-term temperature monitoring necessary. The proposed PA system was able to monitor the thermal condition controlled by switching the CW laser, as shown in Fig. 3(b) [18].

4.3 US/PA bimodal imaging system

To test the thermal effects of irradiating intratumor nanoparticles with a CW laser, 40 μL of a 3-nM AuNRs solution was directly injected into tumors in NOD-SCID mice. Both US and PA images were obtained before and after injection, and displayed in grayscale and pseudocolor, respectively. This bimodal imaging method allows clinicians to specifically identify the locations of tumors and nanoparticles, which aids pretreatment planning. Figures 4(a) and 4(b) show four slices of a mouse tumor before and after nanorod injection, respectively.

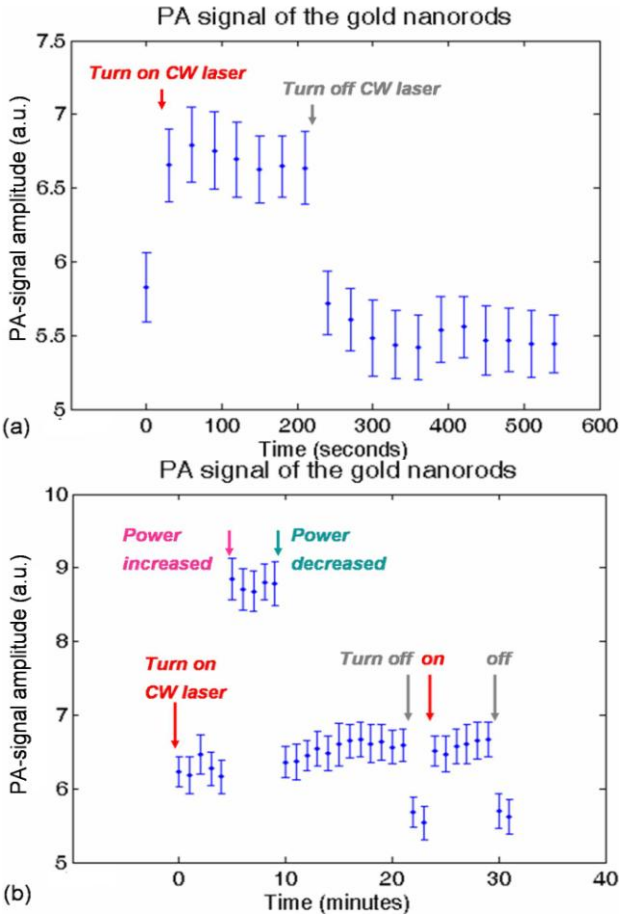

Figure 3. Tests to confirm the performance of the system. Gold nanoparticles were used as the phantom. (a) Short-term changes. (b) Long-term changes. Data are mean and SD values (n = 100). In Fig. 3(b), at the beginning of measurement, the CW laser was turned on, thus the PA signal amplitude kept at high level and then dropped until the CW laser was turned off.

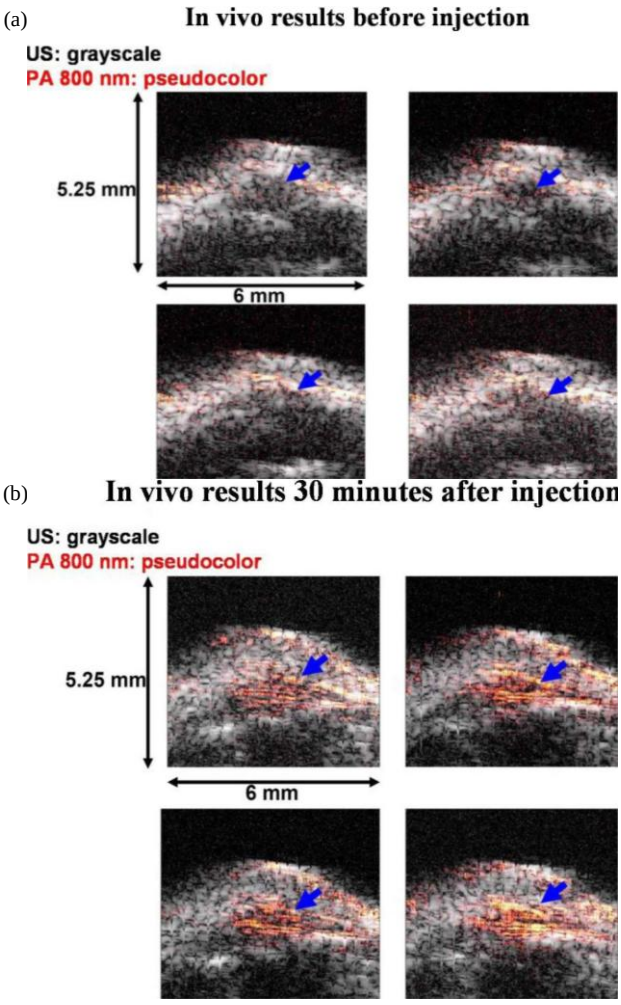

Figure 4. PA signal of nanorods in the tumor. Images obtained (a) before and (b) after injecting nanorods. After injecting the nanorods, a significant PA signal appeared in the hypoechoic portion (blue arrows) of the tumor. The tumor was not heated with CW laser.

4.4 In vivo study with tail-vein injection

Under general anesthesia with isoflurane, 40 μL of 3-nM $AuNR_{800}$-RGD4C was injected into the tumor, which was then irradiated by a 800-nm CW laser at 660 mW for 5 minutes. A pulsed laser operating at 800 nm with a pulse energy of 2.5 mJ was employed to generate the PA signal. The local temperature near the ROI was recorded with a fine-needle thermocouple that was not irradiated by the CW laser. The affinity for trapping RGD-conjugated nanorods was higher for the tumor than for the surrounding normal tissue.

Thirty minutes after the nanorods were injected, the tumor was irradiated by a CW laser and PA images were obtained. Four groups of PA signals were analyzed (Fig. 5) [18]:

1. No nanorods injected / no CW laser irradiation. PA signal amplitude: mean (μ) = 0.017, standard deviation (σ) = 0.005.
2. No nanorods injected / CW laser irradiation: μ = 0.014, σ = 0.003.
3. Nanorods injected / no CW laser irradiation: μ = 0.173, σ = 0.079, T^* = 26.4℃.
4. Nanorods injected / CW laser irradiation: μ = 0.529, σ = 0.124, T^* = 40.0℃ (T^*: one point temperature of ROI, measured with the fine-needle thermocouple).

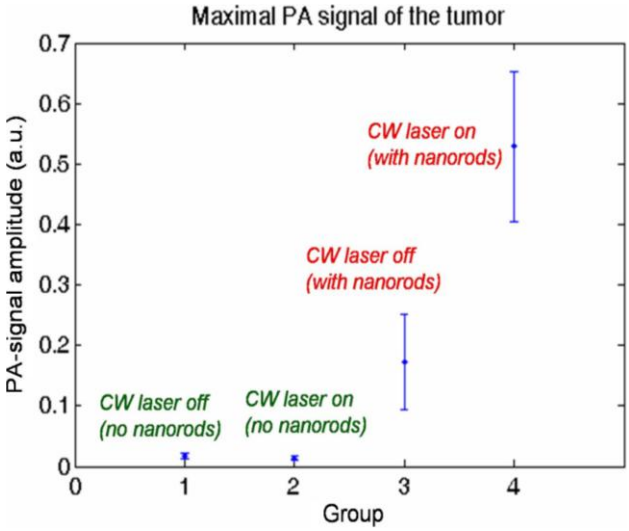

Figure 5. The PA pressure profiles of the tumor in the *in vivo* study of PPTT (n = 3). After heating for 5 minutes with the CW laser, four groups were analyzed: (1) CW laser off without nanorods injected into the tumor, (2) CW laser on without nanorods, (3) CW laser off with nanorods, and (4) CW laser on with nanorods. Data are mean and SD values.

Irrespective of whether CW laser irradiation was present, no significant change in the PA-signal amplitude was evident when nanorods were not injected (Groups 1 and 2). In other words, thermal therapy is difficult to achieve using a CW laser in the absence of AuNRs. In contrast, when nanorods were injected, the CW laser irradiation increased the PA-signal amplitude (Groups 3 and 4). Even without CW irradiation, the PA-signal pressure increased by tenfold in the presence of nanorods (Groups 1 and 3), which is due to the PA response being much stronger from AuNRs than from the intrinsic tissue chromophores. The PA-signal amplitude increased further when both AuNRs were present and CW irradiation was applied (Group 4).

4.5 Temperature mapping

In the proposed system, the temperature is determined by Eqs. (11) and (14). Because soft tissue mainly comprises water, it is assumed that the PA properties of water can be applied when performing temperature mapping of water-based tissues [9].

Based on the thermal properties of water, Grüneisen parameter Γ is plotted as a function of temperature T in Fig. 6. The values of $a = 0.016$ and $b = 0.0046$ (i.e., $d = -3.4783$) can be derived from the data. If the initial temperature and pressure are known, the values of c and temperature T can be obtained.

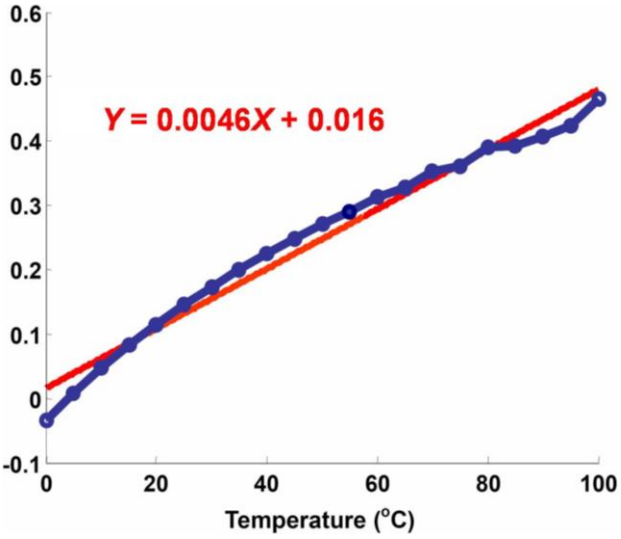

Figure 6. Grüneisen parameter versus the temperature of water. This diagram was based on thermal properties of water.

Using CW laser irradiation at various power levels, the PA profiles of 3-nM solutions of AuNRs and deionized water were collected and analyzed in the phantom study. When subjects with an initial temperature of $T_0 = 22.3$℃ were heated with a low-power CW laser (720 mW) at 808 nm, thermal images were obtained by calculating $c = 25.7783/P_0(z)$ (Fig. 7(a)). The highest temperatures of the nanorods and deionized water were 38.8 and 31.4℃, respectively. When subjects with an initial temperature of 20.0℃ were irradiated by a high-power CW laser (7.90 W), the thermal images showed that the highest temperatures of nanorods and water were 136.7 and 86.8℃, respectively (Fig. 7(b)). When the 3-nM nanorods solution was heated with a CW laser at powers of 7.90 and 2.73 W, the thermal images showed that the highest temperatures were 136.7 and 51.1℃, respectively (Fig. 7(c)).

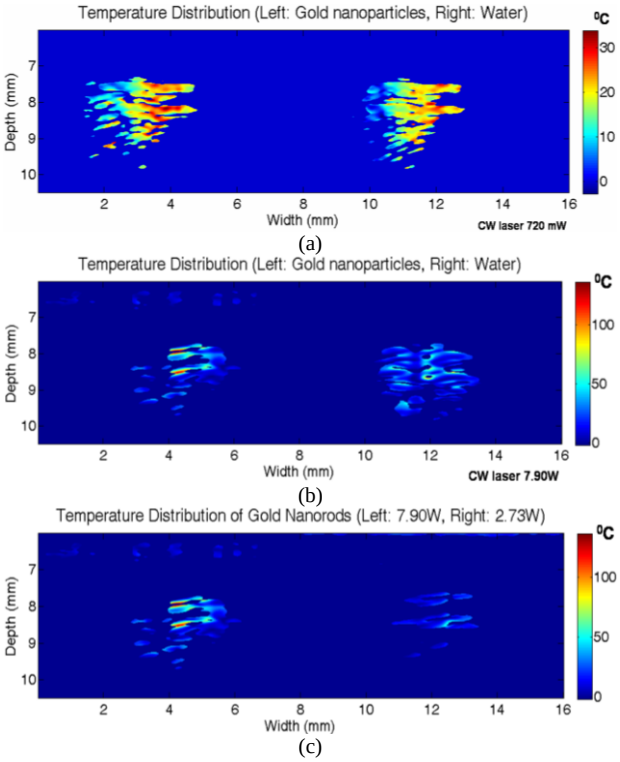

Figure 7. Temperature mapping after heating with the CW laser for 5 minutes. (a) Low-power CW laser irradiation (720 mW) and an initial temperature of 22.3°C (left: AuNR solution, right: deionized water). (b) High-power CW laser irradiation (7.90 W) with an initial temperature of 20.0°C. (c) Heating the 3-nM nanorods solution with a CW laser at 7.90 and 2.73 W.

For treatment purposes, the temperature should be adjusted to be above 42℃ to induce thermal therapy but below 100℃ to prevent carbonization [23]. The thermal expansion coefficient of volume β is a linear function of temperature for soft tissue in the range of 10 to 55℃ [9]. The Grüneisen parameter of water is thus linearly proportional to the temperature, which has been verified experimentally [4]. In our experiments, the temperature range of between 5-95℃ was measured and good linear relationship between the temperature and PA amplitude was found, but the deviation increased with temperature for temperatures higher than 65℃ and decreased with temperature for temperatures lower than 10℃. Nonetheless, for thermotherapy, a linear relationship in the temperature range of 10-65℃ is adequate.

Changes in the speed of sound and the thermal expansion of soft tissue affect temperature mapping. The PA technique for thermal mapping can be applied for a small ROI without such effects. The accuracy increases with decreasing size of the ROI. The thermal image was thus limited to a 3 mm × 5 mm region. For the proposed system, the spatial resolution is 200-300 μm, and depends on the characteristics of the PA imaging system and the associated acoustic frequency. The temperature resolution is 0.1℃.

4.6 *Quantitative thermal imaging for in vivo targeted thermotherapy*

The OECM1 tumor cell line can express large amounts of HER2 protein. $AuNR_{800}$-anti-HER2 nanorods were injected via the tail vein of the mice, and the tumor was irradiated by the CW laser 24 hours later for *in vivo* targeted thermotherapy. The power of the CW laser should not exceed the safety guidelines of ANSI Z136.1 published by the Laser Institute of America (2007). In accordance with these guidelines, a CW laser power density of 320 mW/cm^2 was used to prevent damaging the soft tissue near the tumor. No detectable effects on the skin were observed after thermotherapy.

Combined US and PA images for the four groups of PA signals are shown in Fig. 8. The results were in agreement with those of the phantom study shown in Fig. 5.

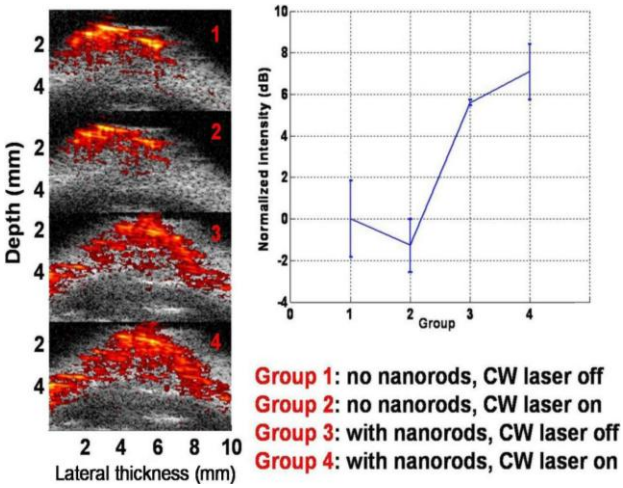

Figure 8. After heating for 5 minutes with the CW laser, combined US and PA images were obtained for the four conditions (Groups 1, 2, 3 and 4). Data are mean and SD values.

The quantitative thermal image obtained after turning the CW laser on 24 hours after injecting AuNRs is shown in Fig. 9. This figure demonstrates that the proposed system is able to perform temperature monitoring for targeted thermotherapy.

The tumor was excised after thermotherapy and examined pathologically. The tumor architecture was destroyed and necrotic tumor cells were present, whereas the nearby hair follicles and intratumor fibroblasts were preserved (Fig. 10). This indicates that targeted thermotherapy is able to selectively kill tumor cells. The peripheral tissue and intratumor noncarcinoma cells were not damaged despite also being irradiated by the CW laser.

5. Conclusions

This study combined US and PA imaging for temperature monitoring and real-time thermal imaging during PPTT. The PA signal can be used to monitor the thermal response of SPR induced by irradiating AuNRs with a CW laser. This bimodal method can provide anatomical information before therapy and be used to monitor temperature changes induced during treatment, thereby improving both safety and efficacy.

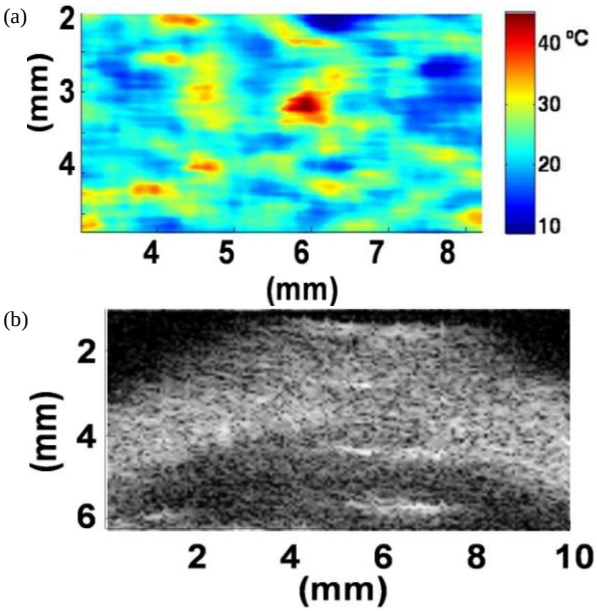

Figure 9. (a) A thermal image of the tumor. (b) The corresponding US image of the tumor. After heating for 5 minutes, and the central temperature of the tumor was above 45°C, indicating the induction of thermal therapy.

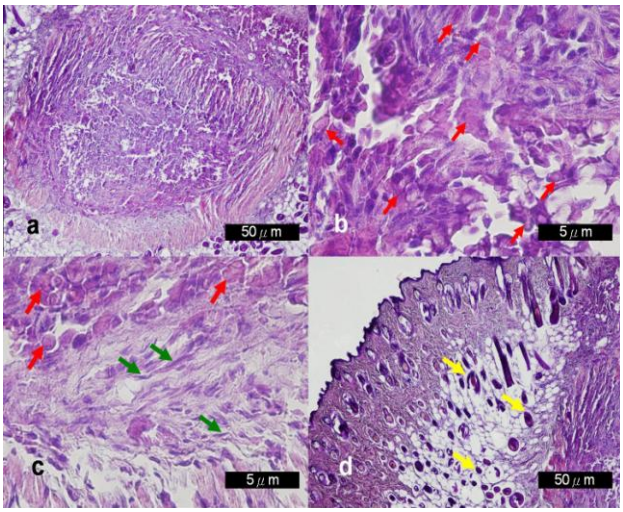

Figure 10. (a) The tumor structure was selectively destroyed by thermotherapy, with preservation of the peripheral tissue. (b,c) Tumor cells showed necrotic changes (red arrows) while fibroblasts within the tumor remained intact (green arrows). (d) The hair follicles near the tumor (yellow arrows) were spared despite being irradiated by the CW laser.

The results show that laser energy is absorbed more effectively by AuNRs than by intrinsic tissue chromophores, which allows nanorods to be used as the contrast agent in PA imaging. Under the conditions specified by the ANSI Z136.1 safety guidelines, it is difficult to induce hyperthermia in the absence of nanoparticles. It was found that targeted thermotherapy can be implemented selectively by using AuNRs conjugated with specific antibodies.

The wavelength at which the absorption of nanorods peaks is determined by their aspect ratio. When the corresponding wavelength is applied by both the pulsed and CW lasers in the proposed system, the nanorods can be used to generate a PA

signal and to monitor the temperature while heating the lesion to hyperthermic conditions. This system is thus suitable for quantitative thermal mapping in AuNR-assisted thermotherapy.

Acknowledgements

The authors thank Dr. Dar-Bin Shieh for providing the NOD-SCID mice, and Dr. Churng-Ren Chris Wang, Chi-Meng Chen, and Carolina Poe for synthesizing the AuNRs and providing the CW laser. The assistance of Yae-lin Sheu, Bao-Yu Hsieh, and Yu-Hsin Wang are also appreciated. We thank Dr. Cheng-Hsiang Hsiao, a pathologist at NTU Hospital, for reviewing the pathology results. The authors are also grateful for support from the National Health Research Institutes, NTU Center for Nano Science and Technology, and NTU Center for Genomic Medicine, and for financial support from the National Science Council under grant NSC 97-3011-P-002-009.

References

[1] X. Huang, P. K. Jain, I. H. El-Sayed and M. A. El-Sayed, "Plasmonic photothermal therapy (PPTT) using gold nanoparticles," *Lasers Med. Sci.*, 23: 217-228, 2008.

[2] T. D. Mast, D. P. Pucke, S. E. Subramanian, W. J. Bowlus, S. M. Rudich and J. F. Buell, "Ultrasound monitoring of in vitro radio frequency ablation by echo decorrelation imaging," *J. Ultrasound Med.*, 27: 1685-1697, 2008.

[3] L. M. Veenendaal, A. Jager, G. Stapper, I. H. M. Borel-Rinkes and R. Van Hillegersberg, "Multiple fiber laser-induced thermotherapy for ablation of large intrahepatic tumors," *Photomed. Laser Surg.*, 24: 3-9, 2006.

[4] I. V. Larina, K. V. Larin and R. O. Esenaliev, "Real-time optoacoustic monitoring of temperature in tissues," *J. Phys. D Appl. Phys.*, 38: 2633-2639, 2005.

[5] R. Seip and E. S. Ebbini, "Noninvasive estimation of tissue temperature response to heating fields using diagnostic ultrasound," *IEEE Trans. Biomed. Eng.*, 42: 828-839, 1995.

[6] C. Simon, P. Vanbaren and E. S. Ebbini, "Two-dimensional temperature estimation using diagnostic ultrasound," *IEEE Trans. Ultrason. Ferroelectr. Freq. Control*, 45: 1088-1099, 1998.

[7] J. Shah, S. R. Aglyamov, K. Sokolov, T. E. Milner and S. Y. Emelianov, "Ultrasound-based thermal and elasticity imaging to assist photothermal cancer therapy: preliminary study," *Proc. IEEE Ultrason. Symp.*, 1029-1032, 2006.

[8] S. Sethuraman, S. R. Aglyamov, R. W. Smalling and S. Y. Emelianov, "Remote temperature estimation in intravascular photoacoustic imaging," *Ultrasound Med. Biol.*, 34: 299-308, 2008.

[9] J. Shah, S. Park, S. Aglyamov, T. Larson, L. Ma, K. Sokolov, K. Johnston, T. Milner and S. Y. Emelianov, "Photoacoustic imaging and temperature measurement for photothermal cancer therapy," *J. Biomed. Opt.*, 13: 034024, 2008.

[10] V. Rieke and K. B. Pauly, "MR thermometry," *J. Magn. Reson. Imaging*, 27: 376-390, 2008.

[11] B. D. Senneville, B. Quesson and C. T. Moonen, "Magnetic resonance temperature imaging," *Int. J. Hyperthermia*, 21: 515-531, 2005.

[12] B. Quesson, J. A. De Zwart and C. T. Moonen, "Magnetic resonance temperature imaging for guidance of thermotherapy," *J. Magn. Reson. Imaging*, 12: 525-533, 2000.

[13] S. Mallidi, G. P. Luke and S. Emelianov, "Photoacoustic imaging in cancer detection, diagnosis, and treatment guidance," *Trends Biotechnol.*, 29: 213-221, 2011.

[14] M. Xu and L. V. Wang, "Photoacoustic imaging in biomedicine," *Rev. Sci. Instrum.*, 77: 041101, 2006.

[15] S. Y. Emelianov, S. R. Aglyamov, A. B. Karpiouk, S. Mallidi, S. Park, S. Sethuraman, J. Shah, R. W. Smalling, J. M. Rubin and W. G. Scott, "Synergy and applications of combined ultrasound, elasticity, and photoacoustic imaging," *Proc. IEEE Ultrason. Symp.*, 405-415, 2006.

[16] G. Schule, G. Huttmann, C. Framme, J. Roider and R. Brinkmann, "Noninvasive optoacoustic temperature determination at the fundus of the eye during laser irradiation," *J. Biomed. Opt.*, 9: 173-179, 2004.

[17] J. Kandulla, H. Elsner, R. Birngruber and R. Brinkmann, "Noninvasive optoacoustic online retinal temperature determination during continuous-wave laser irradiation," *J. Biomed. Opt.*, 11: 041111, 2006.

[18] S. H. Wang, C. W. Wei, S. H. Jee and P. C. Li, "Photoacoustic temperature measurements for monitoring of thermal therapy," *Proc. SPIE*, 7177: 71771S, 2009.

[19] A. A. Karabutov, N. B. Podymova and V. S. Letokhov, "Time-resolved laser optoacoustic tomography of inhomogeneous media," *Appl. Phys. B*, 63: 545-563, 1996.

[20] S. Zitzmann, V. Ehemann and M. Schwab, "Arginine-glycine-aspartic acid (RGD)-peptide binds to both tumor and tumor-endothelial cells in vivo," *Cancer Res.*, 62: 5139-5143, 2002.

[21] Z. F. Su, G. Liu, S. Gupta, Z. Zhu, M. Rusckowski and D. J. Hnatowich, "In vitro and in vivo evaluation of a Technetium-99m-labeled cyclic RGD peptide as a specific marker of alpha(V)beta(3) integrin for tumor imaging," *Bioconjug. Chem.*, 13: 561-570, 2002.

[22] B. R. Line, A. Mitra, A. Nan and H. Ghandehari, "Targeting tumor angiogenesis: comparison of peptide and polymer-peptide conjugates," *J. Nucl. Med.*, 46: 1552-1560, 2005.

[23] M. H. Niemz, *Laser-tissue Interactions: Fundamentals and Applications*, Berlin, Heidelberg: Springer-Verlag, 2003.